Phase-field-crystal modeling of glass-forming liquids: Spanning time scales during vitrification, aging, and deformation

Joel Berry[*] and Martin Grant

Physics Department, McGill University, 3600 rue University, Montréal, Québec H3A 2T8, Canada

(Received 3 September 2013; published 11 June 2014)

Two essential elements required to generate a glass transition within phase-field-crystal (PFC) models are outlined based on observed freezing behaviors in various models of this class. The central dynamic features of glass formation in simple binary liquids are qualitatively reproduced across 12 orders of magnitude in time by applying a physically motivated time scaling to previous PFC simulation results. New aspects of the equilibrium phase behavior of the same binary model system are also outlined, aging behavior is explored in the moderate and deeply supercooled regimes, and aging exponents are extracted. General features of the elastic and plastic responses of amorphous and crystalline PFC solids under deformation are also compared and contrasted.

I. INTRODUCTION

The study of glasses or amorphous solids and the processes by which they form involves a number of long-standing scientific challenges. Understanding the nature of the liquid-to-glass transition from picosecond to kilosecond time scales, including slow relaxations and aging processes, and understanding the atomic origins of the macroscale elastic and plastic properties of disordered solids are two of the ongoing fundamental challenges in this field. The first is strongly linked to the difficulty in describing long time scales with atomic-level theories. The second is a reflection partly of the difficulties faced in applying crystallographic theories of plastic response to atomically disordered materials, but also of the difficulties in accessing plastic flow processes over multiple length and time scales within simulations. In this article, we further examine and develop a modeling approach that aims to describe atomic-level dynamics in glass-forming liquids and glassy solids over multiple time scales. This aim is relevant to the two long-term challenges noted above, thus issues concerning both glass-forming dynamics and solid-state mechanical response are explored.

Phase-field-crystal (PFC) models have been developed over the past decade to describe freezing and melting transitions in liquid-solid systems as well as various nonequilibrium phenomena generally encountered in liquid and solid materials. The method provides atomic-level spatial resolution and naturally incorporates elastic and plastic effects over long time scales [1–3]. PFC free energy functionals can be viewed as a simple class of classical density functional theory [3], which has been widely used to study freezing and glass formation [4–21]. Freezing in typical PFC and density functional theories generally occurs through first-order classical or spinodal nucleation processes [2,22], including cases in which the resulting solid is amorphous [22–24]. Freezing behavior consistent with established glass transition phenomenology has been predicted for various nonlinear classes of classical density functional theory [15–18], but these predictions have

not been confirmed numerically because the full density functional description is relatively inefficient and unstable in terms of numerical, grid-based solutions. PFC models, by comparison, are highly efficient and stable numerically and, thus, offer an alternate means of examining the glass-forming dynamics generated by density-functional-type models. Our recent numerical simulations have confirmed that when strong nonlinear terms which suppress crystallization are included in the free energy functional [25], one such class of models does exhibit freezing behavior consistent with a glass transition.

While these recent findings may open pathways to more detailed studies of glass-forming dynamics in coarse-grained atomistic models, many questions concerning the general model features that drive glass formation, the range of time scales that can be described, and the properties of the low-temperature glass states remain unanswered. To our knowledge, the mechanical response of amorphous solids has not been examined at all with PFC models. Plastic flow and relaxation in glasses occur across a range of length and time scales and lead to phenomena such as shear banding, shear-induced melting, and shear-induced order—processes often involving behaviors unique to atomically disordered solids. Difficulties arise in comparing, for example, molecular dynamics simulation results of plastic deformation with experiments due to the typically large disparity in strain rates. Thus examination of these processes over long time scales and at lower strain rates using the PFC approach seems a potential route to new insights as well.

The standard monatomic PFC free energy functional has the form

$$F = \int d\vec{r} \left\{ \frac{n}{2}[r + (q^2 + \nabla^2)^2]n + \frac{1}{4}n^4 \right\}, \quad (1)$$

where $n \to n(\vec{r},t) + \bar{n}$ is the scaled time-averaged number density of particles, $\bar{n}$ is the average number density, r is related to the liquid bulk modulus, and q sets the equilibrium distance between particles (see Refs. [2,3] for further discussion of how these parameters relate to material properties).

The primary system studied in this work is a binary PFC mixture with dimensionless Helmholtz potential given by

$$F = \int d\vec{r} [f_{AA} + f_{BB} + f_{AB}], \quad (2)$$

————
[*]Current address: Department of Mechanical and Aerospace Engineering, Princeton University, Princeton, NJ 08544, USA; jmberry@princeton.edu

where

$$f_{ii} = \frac{n_i}{2}\left[r_i + \left(q_i^2 + \nabla^2\right)^2\right]n_i + \frac{1}{4}n_i^4 + H_i\left(|n_i|^3 - n_i^3\right) \quad (3)$$

and

$$f_{AB} = \frac{n_A}{2}\left(q_{AB}^2 + \nabla^2\right)^2 n_B + \frac{r_{AB}}{2}n_A^2 n_B^2. \quad (4)$$

In this notation $i = A$ or B, and $n_i, \bar{n}_i, r_i, q_i$ are species-specific parameters analogous to those of Eq. (1). The parameter q_{AB} sets the distance between A and B particles, and H_i and r_{AB} are additional constants. The terms multiplied by H_i discourage $n_i < 0$ and are the distinguishing feature of the vacancy PFC model [26,27]. A strong $n_i \geqslant 0$ cutoff enforces the physical interpretation of n_i as a constrained number density and, in doing so, produces a range of highly nonlinear responses. The resulting solutions take the form of interacting time-averaged density peaks in both the liquid and the solid phases, with local regions of $n_i \simeq 0$ representing unoccupied, or vacancy, sites.

The dynamics of the coarse-grained density fields n_i are approximated either by a nonlinear stochastic diffusion equation of the form

$$\frac{\partial n_i}{\partial t} = \nabla^2 \frac{\delta F}{\delta n_i} + \sqrt{M_i}\eta_i \quad (5)$$

or by an inertial-diffusive equation of motion that includes both "fast" wave-like processes and "slow" dissipative processes,

$$\frac{\partial^2 n_i}{\partial t^2} + B_i \frac{\partial n_i}{\partial t} = c_i^2 \nabla^2 \frac{\delta F}{\delta n_i} + \sqrt{M_i}\eta_i. \quad (6)$$

Here t is dimensionless time, η_i is a Gaussian stochastic noise variable with $\langle \eta_i(\vec{r}_1,t_1)\eta_i(\vec{r}_2,t_2)\rangle = \nabla \cdot \nabla \delta(\vec{r}_1 - \vec{r}_2)\delta(t_1 - t_2)$, and c_i, B_i, and M_i are constants related to the sound speed, damping rate, and temperature, respectively. An explicit Euler finite-difference algorithm was used to solve Eq. (6) in three dimensions with periodic boundary conditions. Dynamic relaxations were characterized largely in terms of the intermediate scattering functions,

$$F_{ij}(q,t) = \frac{\langle \delta n_i(q,0)\delta n_j^*(q,t)\rangle}{F_{ij}(q,0)}, \quad (7)$$

where q is wave number and $\delta n_i = n_i(\vec{r},t) - \bar{n}_i$. Static structural correlations were also analyzed using the structure factor of most probable atomic positions, $S_{ij}^P(q) = \langle \delta n_i^P(q)\delta n_j^{P*}(q')\rangle$, where $\delta n_i^P(r)$ is a binary map of the positions of the local number density peaks.

Unless otherwise specified, all quenching simulations were performed as follows. First, the liquid is equilibrated at a temperature T_i until all diagnostics reach a steady state, then the system is quenched to a final temperature T at some rate $\dot{T}$. The system is held at this final T until the free energy reaches a steady state, at which point the measurement of $F_{ij}(q,t)$ is initiated. Data from several such simulations are then averaged together to obtain the final results.

Temperature enters PFC models through all coefficents in the free energy and, if stochastic thermal noise is considered, through the standard relation between noise amplitude and T. Though all coefficents are, in principle, temperature dependent, we employ the common approximation that the second-order term in n, which has leading temperature

dependence, is the lone nonstochastic temperature variable. Thus we define $T = r_i + 1$. The stochastic contribution to T, which we consider independently of r_i, should obey $T \sim M_i$. Thus we further define $T = T_p M_i$, where T_p is an arbitrary constant. In a given simulation, we take either $T = r_i + 1$ with M_i constant or $T = T_p M_i$ with r_i constant. In Sec. II the choice of T parameter is specified for each data set, while only the stochastic definition is employed in Secs. III and IV.

The remainder of this article is arranged as follows. In Sec. II results from analyses of freezing dynamics in a variety of PFC and density functional theories are summarized. By comparing and contrasting the observed behaviors, we isolate two essential model features sufficient for generating glass transition dynamics consistent with known phenomenology. In Sec. III a time scaling procedure is outlined which attempts to optimize the PFC description toward increasingly slow time scales as the glass transition temperature T_g is approached from above. Qualitative agreement with known relaxation phenomenology is obtained across 12 orders of magnitude in time using this approach. Finally, in Sec. IV, the preliminary results reported in Ref. [25], which demonstrate agreement between PFC simulations and the central predictions of mode coupling theory for liquid dynamics in the moderately super-cooled regime, are expanded upon. New results concerning the equilibrium phase behavior of this model, aging properties exhibited during the intermediate and late stages of the glass transition, and the elastic and plastic responses of the stabilized glassy solids are presented.

II. ELEMENTS OF GLASS-FORMING DYNAMICS IN PFC AND DENSITY FUNCTIONAL MODELS

The standard PFC formulation [2] generates a first-order nucleation-driven freezing transition in three dimensions, the strength of which decreases as the transition point approaches the liquid spinodal boundary [22]. The resulting inhomogeneous solid phase may be crystalline, amorphous, or a combination of both, but fundamental elements of the liquid to amorphous solid transition dynamics and thermodynamics are inconsistent with known properties of the glass transition. We may therefore presume that important elements of the atomic cage-level physics of highly nonequilibrium glass-forming liquids are not fully captured by the simplest PFC formulations. One modified PFC model was recently shown by us to capture the dynamics of glass formation in considerable detail [25], but the minimal ingredients required for such behavior and their connections with the fundamental physics of the transition have not yet been clarified.

We have attempted to isolate physically motivated modifications to the basic PFC description that generate the correct glass transition dynamics. By examining the nature of the freezing transitions in a wide range of PFC models as nonlinearities are introduced into the original PFC functional and as alternate equations of motion are employed, we have concluded that two additional model elements provide conditions sufficient for the appearance of a glass transition in PFC-type models. The first is a source of strong local or nonlocal nonlinearity in the free energy, such as a vacancy PFC cutoff [the last term in Eq. (3)] or a term that suppresses A-B overlap [the last term in Eq. (4)]. Such terms can generate

sufficient caging to suppress crystallization and produce a fragile glass transition with a Vogel-Fulcher divergence in the primary structural relaxation time. The second essential model element is an equation of motion describing two or more time scales, such as Eq. (6). Such dynamic equations, in combination with strongly nonlinear functionals, are able to generate two-step relaxation functions in the supercooled liquid phase with the basic features predicted by the mode coupling theory of glass formation. These two sufficient conditions do not necessarily apply to all glass-forming systems or models thereof, but we believe that their physical interpretation in terms of caging mechanisms and dynamic processes with multiple characteristic time scales implies some degree of generality beyond just the class of models considered here.

A. Monatomic liquids

Monatomic systems are known from experiments and computer simulations to be poor glass formers in general. Some elements of the standard glass transition phenomenology may be observable with very rapid quenches and/or over relatively short time periods, but instability to crystallization is typically manifested at later times. Simple monatomic PFC-type models quenched using Eq. (5) or related nonlinear diffusive equations of motion (such as that studied in Ref. [16]) can produce disordered solid structures, but generally via a discontinuous, nucleation-driven freezing transition and with relatively simple relaxation processes tending to persist. More promising results in terms of continuous vitrification are obtained for standard monatomic PFC liquids evolved using the inertial-diffusive equation of motion, Eq. (6). Such systems do seem to exhibit a nearly continuous transition from liquid to glass, with signs of plateauing correlators, but they generally suffer from rapid crystallization as in the noninertial case. Heavily oscillating relaxation functions also tend to appear under the conditions required for continuous monatomic glass formation.

Stronger nonlinearities in the form of either three-body correlations [28] or disordered external pinning potentials (quenched disorder) further promote and stabilize glass-like strucutres in two dimensions, where they otherwise tend to be unstable. Both approaches nonetheless continue to generate discontinuous freezing behaviors when Eq. (5) is employed, unless the strength of the quenched disorder is explicitly increased in a continuous fashion. Neither approach is therefore satisfactory as a means of studying the dynamics of structural glass formation.

Glass-like structures in monatomic systems are therefore generally accessible and often quite stable at low T, but a comprehensive monatomic glass former that does not crystallize at intermediate temperatures and maintains consistent dynamic and thermodynamic behavior does not seem readily obtainable within the basic PFC formalism. The monatomic vacancy PFC liquid described in Ref. [25] is relatively close to reaching these goals but is also inherently unstable to crystallization over typical simulation time scales at intermediate temperatures. These behaviors are consistent with expectations for monatomic liquids.

B. Binary liquids

Two-component systems with an appropriately chosen size ratio between atomic species are often used as model systems for glass formation. A modest size difference between the two atom types can greatly suppress crystallization and generate a clear glass transition in the deeply supercooled liquid regime. As an illustration, we show here that a model containing two diffusively relaxing fields with slightly different equilibrium periodicities and a purely repulsive coupling is suffcient for the appearance of a structural glass transition. This minimal binary PFC model is composed of two standard monatomic functionals for A and B atoms, coupled only by a local repulsive interaction term. It is given by Eq. (2) with

$$f_{ii} = \frac{n_i}{2}\big[r_i + \big(q_i^2 + \nabla^2\big)^2\big]n_i + \frac{1}{4}n_i^4 \tag{8}$$

and

$$f_{AB} = \frac{r_{AB}}{2}(n_A + 1)^2(n_B + 1)^2. \tag{9}$$

The constant r_{AB} sets the strength of the mutual repulsion, which discourages peaks in either field from overlapping with those in the other. For simulations with dynamics given by Eq. (5), offset bcc lattices for A and B atoms are easily nucleated upon quenching with $q_A = q_B$. When $q_B/q_A = 4/5$, the time required to nucleate the equilibrium crystalline structure becomes very large, and the system freezes rapidly but continuously into a disordered solid phase. This is the case for quenches in which $T = T_p M_i$ (nonspinodal) as well as for quenches in which $T = r_i + 1$ (toward a spinodal boundary) as shown in Fig. 1.

The structure factors of the resulting disordered states are glass-like, and the relaxation times diverge smoothly rather than with the sharp increase that indicates a nucleation-driven freezing transition. The relaxation functions do not clearly plateau, but become highly stretched or weakly shouldered (Fig. 1). Thus, other than clearly plateauing correlation functions, this simple coupling of geometrical frustration (due to inefficient crystalline packing) with standard dissipative evolution generates a significant range of glass-forming behaviors. We have also performed simulations using inertial-diffusive dynamics [Eq. (6)] and find that clear plateaus or two-step relaxations emerge as well within this minimal binary model, but some degree of persistent crystallization tends to obscure the transition, as observed for monatomic liquids. Further fine-tuning therefore seems to be required to make this system fully consistent as a model of glass formation, and for this reason the more robust binary vacancy PFC model described in Ref. [25] is the main focus of our present investigations.

III. SPANNING TIME SCALES IN GLASS-FORMING LIQUIDS

As a phenomenological model, the precise physical time scales described by a given set of PFC equations are not known *a priori*. Temporal links with known systems can nonetheless be estimated by equating some measurable dynamic property of a PFC model with that of a known system. Here we propose a method for setting and tuning time scales in PFC models of
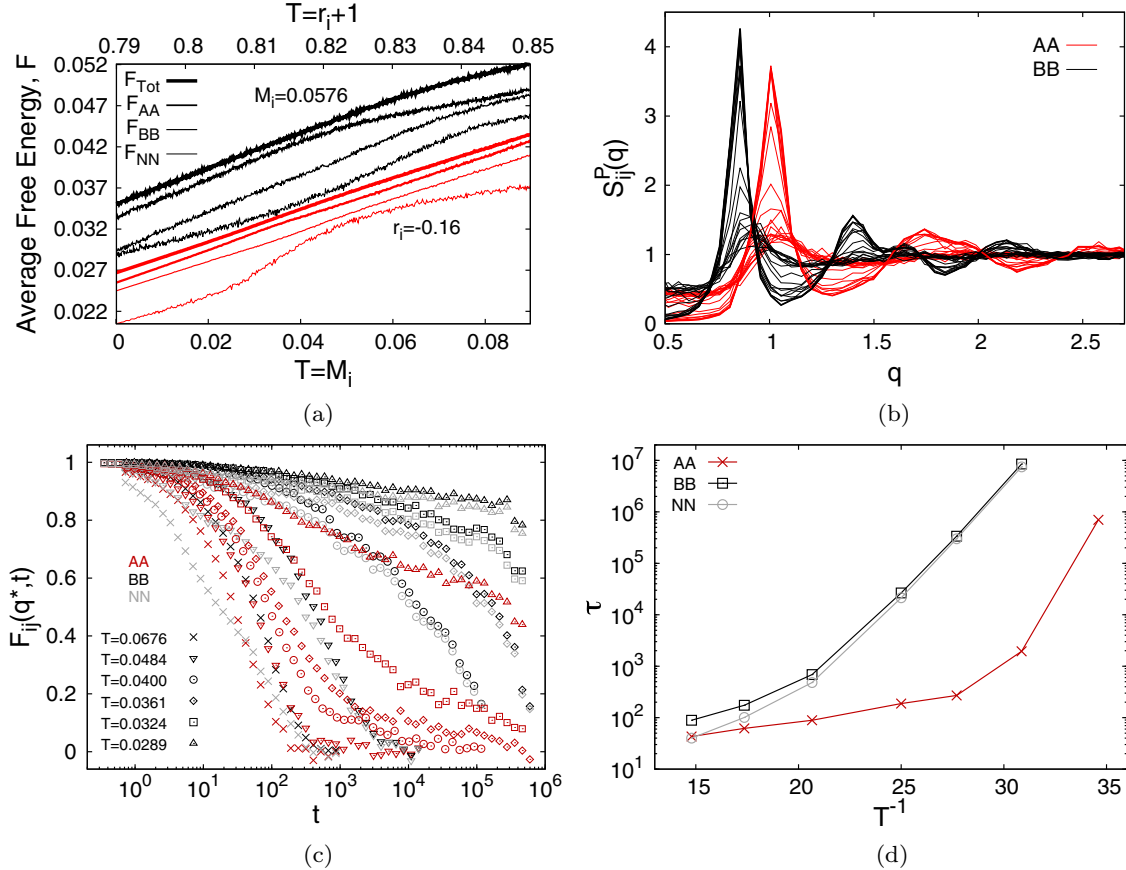
FIG. 1. (Color online) Transition behavior of the minimal mutually repulsive binary PFC glass former given by Eqs. (2), (5), (8), and (9). (a) Free energy vs T during glass formation for both definitions of T ($T = T_p M_i$ with $T_p = 1$, $r_i = -0.16$ and $T = r_i + 1$ with $M_i = 0.0576$). (b) Emergence of glass-like structure factors $S_{ij}^P(q)$ during the $T = M_i$ quench shown in (a) $T_i = 0.09$ to $T = 0$ in $10\,000t$. Curves shown were calculated at $1250t$ intervals, beginning from the initial liquid state and ending with the stable glass state at $50\,000t$. (c) Stretched dynamic correlation functions $F_{ij}(q^*, t)$, where q^* is the wave number of the first peak maximum in $F_{ij}(q,0)$. For all data sets shown, $T = M_i$ with $T_i = 0.0784$ and $\dot{T} = 80(T - T_i)$. (d) Arrhenius plot of diverging relaxation times [$F_{ij}(q^*, \tau) = 1/e$] for $T = M_i$. Unless specified otherwise, $r_{AB} = 1/10$, $q_A = 1$, $q_B = 4/5$, $r_i = -0.16$, $\bar{n}_A = \bar{n}_B = -1/4$, and volume = 128^3. Also, $N = n_A + n_B$.

glass-forming *liquids* which exploits the presence of rapidly separating β and α time scales in the deeply supercooled regime of the glass transition. These two time scales, which are associated with cage-rattling and cage-breaking processes, respectively, are mapped directly onto the two characteristic times described by Eq. (6). These are associated with inertial or wave-like oscillations ($c \to \beta$) and diffusive relaxation ($B \to \alpha$), respectively. An effective dynamic coarse-graining time is then defined in proportion to the parameter B, which sets the relative strength and separation of these two dynamic processes when $c = 1$; $\bar{t} \sim B t_{\text{PFC}}$, where the overbar denotes rescaled or effective coarse-grained time. One may thus describe the normal liquid and moderately supercooled liquid regimes in full detail (to the degree that such liquids are well described by this type of model) by maintaining a sufficiently small separation or strong inertial term and then gradually eliminating the fast processes associated with this term as T_g is approached. In this way the large separation in time between cage-rattling and cage-breaking processes in the deeply supercooled regime near T_g may be invoked to justify increasing the effective coarse-graining time and neglecting the faster processes. We show that this procedure generates strong qualitative agreement with typical experimental data

over 12 orders of magnitude in time for one initial case study.

A. Description of the time-scaling procedure

Relaxations in simple liquids in the high-temperature, non-supercooled regime can be accurately described using either purely diffusive dynamics or an inertial-diffusive equation of motion. Provided that the quasiphonon wave processes are not too underdamped (which leads to unphysical oscillatory relaxations in the liquid), they are unable to propagate over significant distances in the loosely packed liquid phase and do not strongly alter the diffusive relaxations. Thus nearly any B or coarse-graining parameter, appropriately rescaled, should be sufficient in the normal liquid regime.

In the denser, moderately supercooled liquid, longer-lived caging effects begin to appear and contribute to an emerging slow relaxation component or α process in the dynamic correlation functions. In this regime the fast β and slow α processes are distinct but not widely separated in time, and a detailed description appears to require a non-negligible inertial component in the equation of motion. Thus the coarse-graining parameter B should be small enough to capture both

processes on relatively similar time scales, unless only the slow relaxations are of interest.

As T is lowered further and the liquid becomes deeply supercooled, a large separation between α and β time scales emerges. This is a reflection of the increasing time over which a given particle is locally trapped within its cage of neighbors. The highly underdamped, small-B description continues to capture qualitatively both the cage-rattling and the cage-breaking processes but, at very low T, cannot be simulated over long enough times to observe the entire slow α process. As noted, we attempt here to circumvent this problem by invoking a separation-of-scales argument to average out or neglect the shorter time scale and describe only the postplateau α processes. In this way the model dynamics can effectively be "telescoped" across time between the bounds set by the nominal α and β processes. The low-T, late-time results (postplateau, large B) can be transposed onto the higher-T, early-time results (plateau region, small B) to obtain a description of the entire relaxation function even at very low temperatures, near T_g (see Fig. 2).

To summarize, we define $\bar{t} \sim Bt_{\text{PFC}}$ and optimize our description across multiple time scales by tuning B with T as permitted by the physics of glass formation. It is interesting to note that a linear analysis of vacancy diffusion times in this model also generates a scaling proportional to Bt_{PFC} in the long-time limit, supporting the idea that physical times associated with such models are directly scaled by B.

B. Application of the time-scaling procedure

Figure 2 shows the application of these arguments to the binary vacancy PFC glass-forming liquid examined in Ref. [25] [Eqs. (2)–(4) and (6)]. Scaling t with B dilates the measured $F(q, Bt)$ curves such that they span 12 orders of magnitude in time. The small-B results accurately capture the normal and moderately supercooled regimes, including the detailed two-step relaxations, while the large-B results capture the qualitative stretching and rapid divergence of the α relaxation processes. As discussed previously, it is assumed that the large-B results describe only the postplateau relaxations and can therefore be set to begin from the plateau height measured in small-B simulations. The relaxation functions thus rescaled [see Fig. 2(a)] capture the central universal dynamical features of fragile glass-forming liquids as widely observed in experiments [29], mode coupling theory calculations [30,31], and computer simulations [31], though across several additional orders of magnitude in time relative to conventional simulation methods.

A further test of the validity of the $\bar{t} \sim Bt_{\text{PFC}}$ scaling is shown in Fig. 2(b), where the mode-coupling-theory time-temperature superposition principle is applied to the time-scaled data. The detailed mode-coupling-theory functional form is relatively well obeyed by the dynamic correlators for all T and B when time is scaled by B.

To compile the relaxation times of the various curves shown in Figs. 2(a) and 2(b) into one Arrhenius plot with a single effective temperature variable T_{eff}, one must also find a scaling relation between the model temperature T and the variables B and M_i. This is so because of the intrinsic coupling between time and temperature in the stochastic prefactor M_i, which
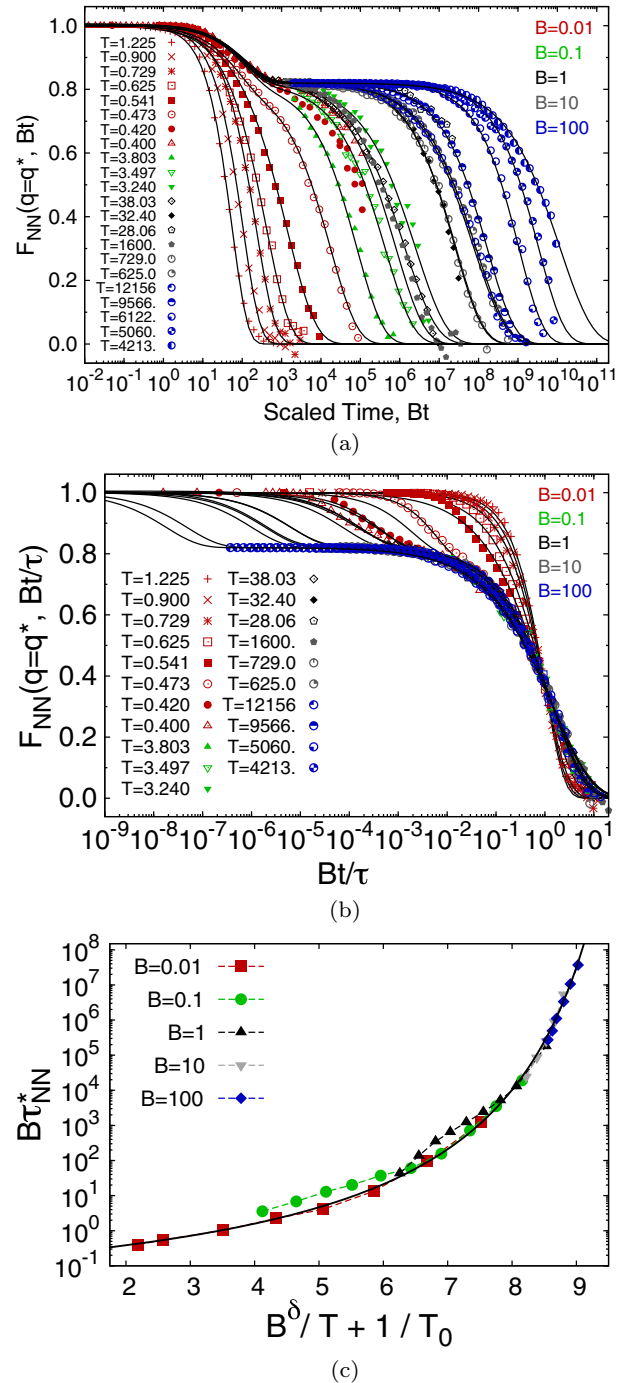

FIG. 2. (Color online) Binary vacancy PFC glass formation in the B-scaled time limit. (a) Dynamic correlators $F_{\text{NN}}(q^*, Bt)$ for various B with time scaled by B. The lines are fits to superimposed stretched exponentials. (b) Same as (a) except with the mode coupling theory $t \rightarrow t/\tau$ scaling, to demonstrate general adherence to the time-temperature superposition principle. The preplateau fit for large B is assumed from the small-B results. (c) Arrhenius plot of scaled relaxation times for various B and the envelope Vogel-Fulcher fit (solid line). τ_{NN}^* is defined as the time at which $F_{\text{NN}}(q^*, t) = 1/e$. The full model is given by Eqs. (2), (3), (4), and (6) with the following parameter values: $\bar{n}_A = \bar{n}_B = 0.075$, $r_i = -0.9$, $q_A = 1$, $q_B = 4/5$, $H_i = 1500$, $q_{AB} = 8/9$, $r_{AB} = 100$, $c_i = 1$, $T_p = 1000$, $\dot{T} = 40(T - T_i)$, $\Delta x = 1$, $\Delta t = 0.025$, and $V = 64^3$, 128^3, or 256^3 (as reported in Ref. [25]).

implies that a definition of time scaled by B necessitates a definition of T that is also rescaled by B in some way. Though it is beyond the scope of this work to derive a formal T rescaling, qualitative approximations can be made in certain limits. For example, the simple scaling $T_{\text{eff}} = T_p M_i / B$ should be applicable in the limit ($M \to 0$, $B \to \infty$). This form follows directly from the time-temperature coupling in the stochastic prefactor M_i noted above. The thermal energy input per time step should increase in proportion to the coarse-graining time $\bar{t}$ [32]; thus if $\bar{t} \sim B t_{\text{PFC}}$ as proposed, then this thermal energy should also increase in proportion to B. The effective temperature must then be $T_{\text{eff}} = T_p M_i / B$ to maintain consistency. Note that the T values needed to induce relaxational dynamics [values displayed in Figs. 2(a) and 2(b)] roughly follow this scaling, with $T = T_p M_i$ increasing nearly in proportion to B, thus maintaining relatively consistent $T_{\text{eff}} = T_p M_i / B$ values. This observed trend is therefore consistent with the proposed $\bar{t} \sim B t_{\text{PFC}}$ time scaling.

This simple scaling breaks down away from the ($M \to 0$, $B \to \infty$) limit for two reasons. For large M_i, the fundamental thermodynamics are altered from those of the $T = 0$ weak-coupling regime, and the bare free energy must be renormalized over the thermal noise to correctly quantify temperature dependencies. This renormalization is difficult to work out rigorously, but we expect that T_{eff} tends to be increased relative to the simple $T_p M_i / B$ scaling when M_i is large. We approximate this effect as $T_{\text{eff}} = T_p M_i / B^{\delta}$, where $\delta \leqslant 1$. As $B \to 0$, strong waves also produce a growing T-like contribution, causing further deviation from the simple scaling. We choose to approximate this second contribution with an added term $1/T_{\text{eff}} = B^{\delta} / (T_p M_i) + 1/T_0(B)$, where the form $1/T_0(B) = a \ln (B) + b$ is found to provide good results when $a = 1.18$, $b = 5.4$, and $\delta = 0.75$. We reiterate that this approximate T rescaling is meant to capture the general effects of large M_i and small B on T_{eff} in a qualitative way only. Nonetheless, all of the relaxation data are brought into accord when this T scaling is applied, with the corresponding τ^* values collapsing toward an envelope function that is well described by a Vogel-Fulcher fit and with the large-B simulations describing the longest times [see Fig. 2(c)]. This too is consistent with the expectations outlined above, in which the small-B description is valid at all T but is limited in time, while the large-B descriptions become valid at sufficiently low T and large times.

These results together, summarized visually in Fig. 2, provide a degree of *a posteriori* justification of the proposed time scaling. The relatively simple picture described here is intended to demonstrate one possible basis for connecting with physical times in systems of this type. One may expect the accuracy of such a description to decrease as the coarse-graining time grows, especially if strong dynamic heterogeneities are present. But the large separation of time scales in these systems ultimately makes a large coarse-graining time necessary within an atomic-level description and, at the same time, serves to justify such a procedure. This approach should therefore generally be most valid for systems in which there are rapidly varying, well-separated dynamic processes, with late-time dynamics dominated by diffusive dissipation.

The preceding discussion is limited to the equations of motion, but one can consider similar coarse-graining arguments

for the free energy functionals as well. For example, since the vacancy PFC approach at least partially builds the explicit vacancy diffusion mechanism back into the model description, its functional must correspond to a smaller coarse-graining time than that of the standard PFC functional. It may therefore be appropriate to employ a highly underdamped vacancy PFC model in the normal and moderately supercooled liquid regimes and not only to increase the dynamic coarse-graining time B in the deeply supercooled regime, but also to employ a standard PFC functional. We have not yet attempted such a procedure.

IV. PROPERTIES OF THE VACANCY PFC MODEL CLASS

Initial results concerning the dynamics of freezing and glass formation in monatomic and binary supercooled vacancy PFC liquids were presented in Ref. [25] and were further rescaled in the previous section. Here we expand on those initial results by presenting new findings related to phase behavior, aging properties, and dynamic mechanical response to applied strains. Both monatomic and binary systems are described by Eqs. (2)–(4) and (6), where $f_{AB} = f_{BB} = 0$ in the monatomic case.

A. Phase behavior

The normal liquid state in vacancy PFC models is a collection of mobile, relatively long-lived density peaks separated by regions of approximately zero density. Additionally, solid vacancy PFC states generally assume density configurations with geometrical features that are not accurately described by the standard sinusoidal one-mode expressions normally applied to PFC solids. For these reasons, analytic calculations of phase diagrams are somewhat more difficult than for standard PFC models, and the three-dimensional case is most readily and accurately treated with numerical simulations. Archer *et al.* [33] have studied the phase behavior of similar models in one and two dimensions. In this study, three-dimensional simulations were initialized with a modified one-mode description of the density field and the free energy was computed after the system reached a steady-state configuration. The modified one-mode description proposed here is given by

$$n(\vec{r}) = [n_{1m}(0 \to 1)]^{g(\bar{n})}, \qquad (10)$$

where $n_{1m}(0 \to 1)$ is the one-mode density expression for a given symmetry, shifted and scaled to span $n = [0,1]$, and $g(\bar{n})$ is the constant power required to achieve a given average density $\bar{n}$. For example, an fcc lattice with $\bar{n} = 9/32$ in this approximation is given by

$$n(\vec{r}) = \left[\tfrac{1}{2} \cos (qx) \cos (qy) \cos (qz) + \tfrac{1}{2} \right]^2, \qquad (11)$$

where q is the equilibrium fcc wave number at a given T. A comparison of the standard one-mode, modified one-mode, and numerically obtained vacancy PFC fcc lattices is shown in Fig. 3(a). Monatomic lattices considered in this study were fcc, bcc, simple cubic, and hexagonally packed rods.

For $\bar{n} = 3/20$, the monatomic liquid state has the lowest observed free energy above $T \simeq 1.32$, while crystalline structures minimize F at lower T. At $T = 4/5$, for example, the fcc lattice has the lowest free energy of those considered. For the
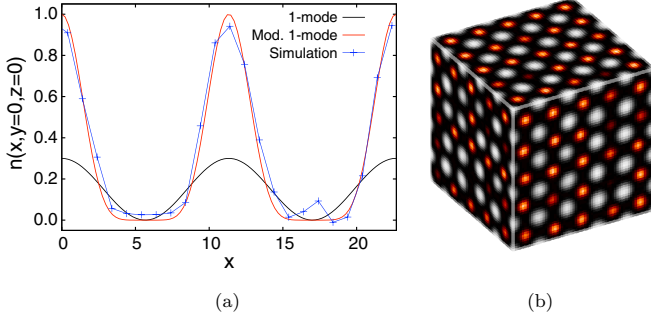
(a)   (b)

FIG. 3. (Color online) (a) A comparison of standard one-mode, modified one-mode, and numerically obtained fcc lattices for the monatomic vacancy PFC model [Eqs. (2)–(4) and (6) with $f_{AB} = f_{BB} = 0$] at $\bar{n} = 3/20$, $T = 4/5$. One-dimensional cross sections shown at $y = z = 0$. (b) The binary $L1_2$ (Cu_3Au) lattice, from a simulation of the binary vacancy PFC model [Eqs. (2)–(4) and (6)] at $\bar{n}_i = 3/40$, $T = 1/10$. n_A is displayed using a black-orange color scheme (grayscale; larger "atoms"), with n_B in grayscale (smaller "atoms").

case of a conserved number density, the liquid-fcc coexistence region spans some range within $4/5 < T < 7/5$, though the precise bounds have not yet been determined. It is sufficient for the present purposes to know that bulk freezing is expected near $T = 33/25$.

Binary vacancy PFC lattices were initialized and evolved in the same manner. Lattices considered in this study are $B1$ (NaCl), $B2$ (CsCl), $B3$ (zincblende), $L1_0$ fcc (CuAu), $L1_2$ fcc (Cu_3Au) and fully phase separated fcc lattices of A and B atoms. The $L1_2$ lattice, for example, with the larger-B atoms located at the unit cell corners, can be written

$$n_A(\vec{r}) = \sum_{k=x,y,z} \left[\frac{1}{2} + \frac{1}{6} \sum_{j=x,y,z} \cos\left[qj + \pi(\delta_{jk} - 1)\right] \right]^{g_A(\bar{n})},$$

$$n_B(\vec{r}) = \left[\frac{1}{2} + \frac{1}{6}(\cos(qx) + \cos(qy) + \cos(qz)) \right]^{g_B(\bar{n})},$$
(12)

where, for example, $g_A(9/16) = 3$ and $g_B(3/16) = 3$ [see Fig. 3(b)].

For $\bar{n}_i = 3/40$, the liquid state has the lowest measured free energy for $T \gtrsim 3/4$, while the $L1_2$ lattice has the lowest free energy of all lattices considered for $1/10 \leqslant T \lesssim 3/4$. The observed variation in stability of the $L1_2$ crystal suggests that its solidus lies near $T = 3/5$ and its liquidus near $T = 7/10$. The $L1_2$ lattice is the only of those examined with an average free energy lower than that of a typical disordered solid. An $L1_2$ crystal will ideally contain three A atoms for each B atom if no vacancies are present, while the present system contains equal numbers of A and B atoms. If we assume that every B site is always occupied, this would imply that only one of three A sites can be occupied at any instant to realize this nonstoichiometric structure. This inconsistency can be corrected by independently varying the n_i^4 coefficients in f_{ii} to adjust the amplitudes of A and B density peaks such that a stiochiometric configuration minimizes the free energy.

B. Aging properties

Glasses, and systems out of equilibrium in general, are known to display aging behaviors. Their physical properties vary with time as the system evolves irreversibly through phase space toward lower energy configurations. The intermediate scattering function can be generalized to include a waiting time t_w, which becomes important out of equilibrium:

$$F(q,t_w + t,t_w) = \langle \exp\{iq[n(t_w + t) - n(t_w)]\}\rangle. \quad (13)$$

Such relaxation functions can often be separated into two components,

$$F(q,t_w + t,t_w) = F_{\text{fast}}(q,t) + F_{\text{aging}}(q,t/t_w^\mu), \quad (14)$$

where F_{fast} contains rapid processes, which do not depend on t_w, and F_{aging} contains the slower processes, which do depend on t_w and often obey a simple t/t_w^μ scaling, where $\mu \leqslant 1$ is called the aging exponent.

The observed effect of waiting time t_w on the supercooled PFC liquid relaxations is shown in Fig. 4. Equilibrated samples were quenched instantaneously from $T = 9/10$ to the indicated T, and $F_{ij}(q,t_w + t,t_w)$ measured for $t_w = 10^0$ to 10^6
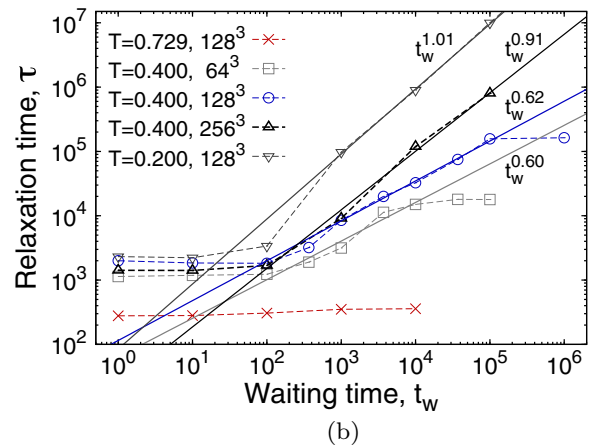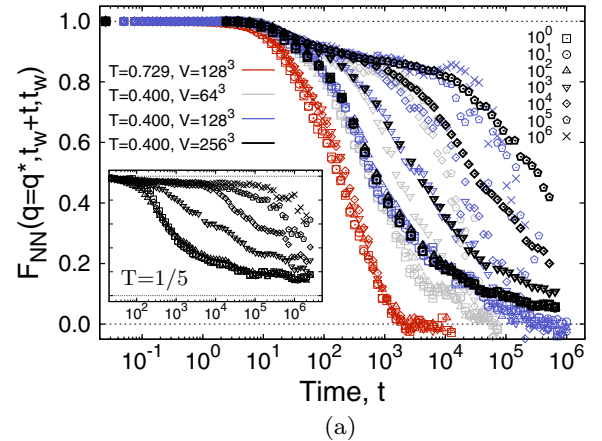

(a)

(b)

FIG. 4. (Color online) Aging behavior in the underdamped binary vacancy PFC supercooled liquid given by Eqs. (2)–(4) and (6). Samples quenched from $T = 9/10$ and monitored after various waiting times t_w. (a) $F_{\text{NN}}(q^*,t_w + t,t_w)$ for various t_w, T, and system sizes. Inset: Data for $T = 1/5$ glass. (b) Measured relaxation time vs t_w showing the various scalings with t_w. Parameter values are the same as those in Fig. 2 with $B = 0.01$ and $T_i = 1.225$.

by powers of 10. The normal liquid at $T = 0.729$ exhibits only very minor signs of aging, even for values of t_w much smaller than the equilibrium relaxation time. This suggests that the free energy landscape in the normal liquid state is relatively flat, such that any initial liquid-like state will already be close to equilibrium and will very rapidly lose any small initial history dependence.

At $T = 2/5$, well into the glass-like regime, clear aging effects emerge for all values of t_w smaller than the structural relaxation time. The general behavior is very similar to that observed in molecular dynamics simulations [34] and colloidal experiments [35]. There is an initial range of small t_w values for which the relaxation functions show little or no t_w dependence. Above this T-dependent lower cutoff, a systematic t_w dependence becomes apparent, with very good adherence to the predicted $F_{fast} + F_{aging}$ decomposition. Short time scales remain independent of t_w, while slow relaxations scale quite well with t/t_w^μ. The measured values of μ are in the range of 0.6 to 1.0, with possible modest dependences on system size and T.

The t_w scalings break down at large t_w as the steady metastable relaxation function is eventually obtained and aging ceases. For system sizes smaller than the dynamic correlation length, the steady metastable relaxation function is size dependent, while no size dependence is observed for systems larger than ξ_D at a given T. Thus finite-size effects are present in the $T = 2/5$ and $T = 1/5$ data for all accessible system sizes. Another interesting feature of the low-T data is the long-time tail that appears for small t_w. This seems to be a reflection of the sudden introduction of slow processes and significant local trapping. The slow time scale is immediately evident in the relaxations for all t_w but takes some finite amount of time to reach a steady state as the system settles into the new, more restrictive free energy landscape.

C. Elastic and plastic responses of glasses and crystals

Another potential application for models of this type is investigation of glassy structures under low-strain-rate deformation where complex dynamic processes spanning a range of length and time scales often emerge. Our present aim is simply to demonstrate that fundamental differences in mechanical response between crystals and glasses are naturally captured by the PFC description due to the atomistic nature of $n(\vec{r})$.

Figure 5 shows a comparison of glass and crystal energies under various constant applied shear rates. The crystalline systems deform elastically and linearly until a yield point is approached and a transition to relatively steady plastic flow occurs. The crystal, which initially contains no defects, exhibits two types of yielding behavior. At high shear rates, stress relief occurs through slipping of atomic layers near the surfaces at which shear is applied. At lower shear rates, stress relief occurs through rapid disordering of some portion of the system (see Fig. 5), followed by a steady-state flow regime in which crystalline regions remain elastic and amorphous regions flow plastically. The volume fraction of the amorphous region first increases as the shear rate is lowered and layer slipping becomes less preferable. Eventually this trend reverses at very low shear rates. If the crystal is
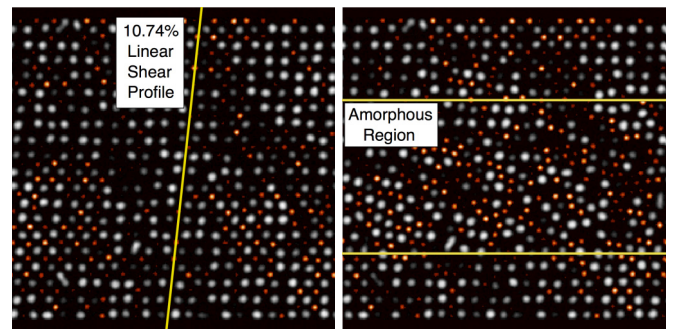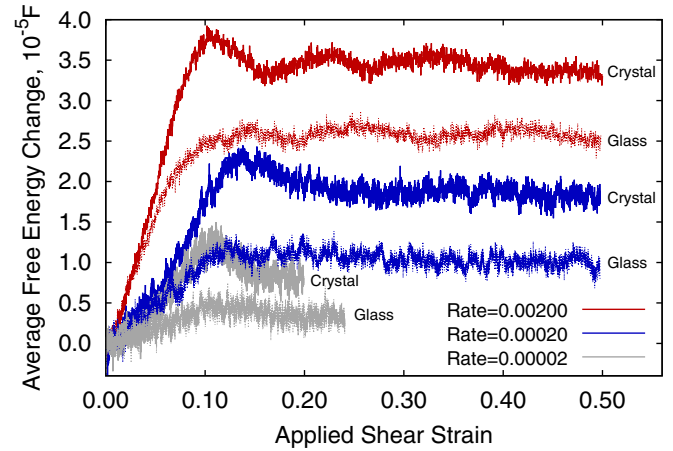

FIG. 5. (Color online) Top: Average free energy vs shear strain for perfect $L1_2$ crystals (thick solid lines) and glassy systems (dotted lines) in the underdamped binary vacancy PFC model [Eqs. (2)–(4) and (6)]. Results for various constant shear rates are shown. Bottom: Cross sections of an $L1_2$ crystal at 10.74% and 19.85% applied strain, under shear rate $0.00002/t$. Parameters are the same as those used in Ref. [25] ($\bar{n}_i = 3/40$, etc.), with $B_i = 0.01$, $T = 1/5$, and volume $= 256^3$. n_A is displayed using a black-orange color scheme (grayscale; larger "atoms"), and n_B is in grayscale (darker; smaller "atoms").

given some initial defect density, the tendency toward bulk disordering is reduced and a jerkier regime of plastic flow is observed, as defect motion alone is able to relieve much of the applied stress.

In glassy systems, reversible elastic deformation at small applied strains is followed by a gradual crossover to irreversible plastic deformation at larger strains, toward a strain threshold above which unbounded steady-state plastic flow occurs. Generally, no pronounced yield point is observed. These behaviors are consistent with general expectations for plasticity in amorphous materials, as are the intermittent fluctuations in the steady-state regime, which seem suggestive of avalanche-type plastic events.

The apparent shear moduli of the aging glasses are smaller than those of the perfect crystal and also exhibit a greater rate dependence. A strong dependence of the state of the system on the history of past deformations is also apparent. Unlike the crystal, the aging glass systems exhibit a crossover from viscous to elastic response as the shear rate is increased. If the structural relaxation time of the glass is shorter than the time required to translate the sheared surface of the sample some meaningful distance, say 1 a.u., then the mechanical energy
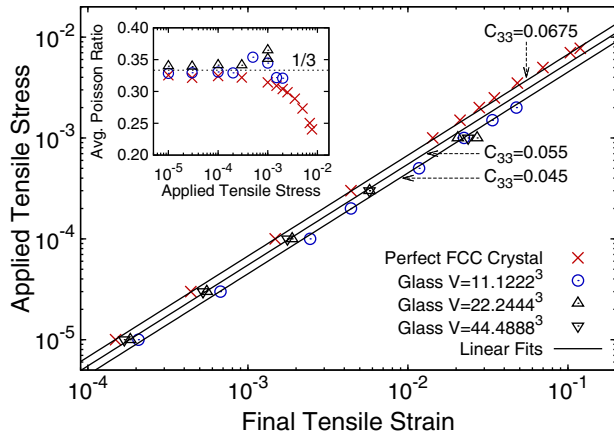
FIG. 6. (Color online) Constant stress mechanical response of standard PFC glasses and fcc crystals [Eqs. (1) and (5)]. Linear stress-strain behavior eventually gives way to nonlinear elastic behavior and then plastic flow at high stresses and strains. Inset: Measured Poisson ratios of glass and crystal systems vs applied stress. Parameters are the same as those used in Ref. [37]: $n_0 = -0.48$, $r = -0.63$, $M_i = 0$, $\Delta x = 0.092\,685 = a_{fcc}/20$. The system sizes in terms of number of atoms are roughly 864, 6912, and 55 296 for volume $= 11.1222^3$, 22.2444^3, and 44.4888^3, respectively.

input is dissipated rather than stored as elastic energy. Thus the response is viscous, and in contrast to the crystal, the peak free energy change appears to approach 0 along with the shear rate, as shown in Fig. 5. If the structural relaxation time is longer than the characteristic shear time, then the mechanical energy input can be stored as elastic energy, and the response is elastic.

The mechanical response of glasses in standard, nonvacancy PFC models [1,2] is somewhat different. The rapid cage-rattling process is absent and the structural relaxation time of the glassy state becomes extremely large (unless M_i is large). The response to a slow, small deformation is therefore always elastic, in contrast to the viscous response of the moderate-T-vacancy PFC glass. Standard PFC crystals and glasses exhibit similar linear elastic behavior for stresses $\lesssim C_{ii}/20$ and similar Poisson ratios of $\sim 1/3$, as shown in Fig. 6. The elastic moduli and the yield stresses of the glasses are generally smaller than those of the perfect crystal, as shown in Fig. 6, though the glass moduli become somewhat larger as the system size is increased.

The general features of the mechanical response observed in these simulations of perfect crystals and glasses suggest that many elements of plasticity in amorphous materials can be captured by PFC-type descriptions. The detailed nature of these elements will require closer analysis to determine whether the mechanisms at work and the local correlated dynamics that emerge are consistent with those observed in other atomistic simulations. Though amorphous plasticity and defect-mediated crystal plasticity exhibit a mix of differences

and similarities, it will be interesting to see whether PFC studies of the mechanics of amorphous materials keep pace with progress already made in terms of crystal plasticity [36–38].

V. CONCLUSIONS

The dynamics of glass-forming PFC liquids have been examined across a large range of time scales and shown to exhibit the same central features observed in many simple glass-forming systems. Two essential model components have been identified as sufficient for generation of a glass transition within PFC-type descriptions. The first is a source of strong nonlinearity in the free energy that generates sufficient caging to suppress crystallization and produce a fragile glass transition with a Vogel-Fulcher divergence in the primary structural relaxation time. The second is an equation of motion describing two or more time scales, which will generate two-step relaxation functions in the supercooled liquid phase with the basic features predicted by the mode-coupling theory of glass formation.

These central dynamic features are qualitatively reproduced across 12 orders of magnitude in time after a physically motivated time scaling is applied to our previously reported simulation results. Other new aspects of the equilibrium phase behavior of the simple binary model system have also been outlined. Aging behavior has been explored in the moderate and deeply supercooled regimes, and the extracted aging exponents are consistent with those observed in other glass-forming systems. General features of the elastic and plastic responses of amorphous and crystalline PFC solids under deformation have been compared and contrasted as well. Amorphous systems exhibit lower elastic moduli and less pronounced yield behavior than perfect crystalline systems, with an initial elastic response crossing over smoothly into a regime of globally steady but locally heterogeneous plastic flow. The overall mechanical response is viscoelastic, with a crossover from viscous to elastic behavior at frequencies above roughly the inverse structural relaxation time of the glassy state. We hope that these findings will prove useful both as a general guide to constructing efficient PFC models with realistic glass-forming properties and as an illustration of the range of time scales and processes that can be accessed by such models.

[1] K. R. Elder, M. Katakowski, M. Haataja, and M. Grant, Phys. Rev. Lett. **88**, 245701 (2002).

[2] K. R. Elder and M. Grant, Phys. Rev. E **70**, 051605 (2004).

[3] K. R. Elder, N. Provatas, J. Berry, P. Stefanovic, and M. Grant, Phys. Rev. B **75**, 064107 (2007).

[4] Y. Singh, Phys. Rep. **207**, 351 (1991).

[5] G. Kahl and H. Löwen, J. Phys.: Condens. Matter **21**, 464101 (2009).

[6] H. Löwen, Phys. Rep. **237**, 249 (1994).

[7] D. Oxtoby, Annu. Rev. Mater. Res. **32**, 39 (2002).

[8] M. Haataja, L. Gránásy, and H. Löwen, J. Phys.: Condens. Matter **22**, 360301 (2010).

[9] Y. Singh, J. P. Stoessel, and P. G. Wolynes, Phys. Rev. Lett. **54**, 1059 (1985).

[10] C. Dasgupta, Europhys. Lett. **20**, 131 (1992).

[11] C. Dasgupta and S. Ramaswamy, Physica A **186**, 314 (1992).

[12] V. Lubchenko and P. G. Wolynes, Annu. Rev. Phys. Chem. **58**, 235 (2007).

[13] U. M. B. Marconi and P. Tarazona, J. Chem. Phys. **110**, 8032 (1999).

[14] A. J. Archer and R. Evans, J. Chem. Phys. **121**, 4246 (2004).

[15] A. Andreanov, G. Biroli, and A. Lefèvre, J. Stat. Mech. (2006) P07008.

[16] B. Kim and K. Kawasaki, J. Phys. A: Math. Theor. **40**, F33 (2007).

[17] A. J. Archer, J. Chem. Phys. **130**, 014509 (2009).

[18] A. J. Archer, J. Phys.: Condens. Matter **18**, 5617 (2006).

[19] U. M. B. Marconi and P. Tarazona, J. Chem. Phys. **124**, 164901 (2006).

[20] U. M. B. Marconi and S. Melchionna, J. Chem. Phys. **126**, 184109 (2007).

[21] U. M. B. Marconi, P. Tarazona, F. Cecconi, and S. Melchionna, J. Phys.: Condens. Matter **20**, 494233 (2008).

[22] J. Berry, K. R. Elder, and M. Grant, Phys. Rev. E **77**, 061506 (2008).

[23] G. I. Tóth, T. Pusztai, G. Tegze, G. Tóth, and L. Gránásy, Phys. Rev. Lett. **107**, 175702 (2011).

[24] A. J. Archer, M. J. Robbins, U. Thiele, and E. Knobloch, Phys. Rev. E **86**, 031603 (2012).

[25] J. Berry and M. Grant, Phys. Rev. Lett. **106**, 175702 (2011).

[26] P. Y. Chan, Ph.D. thesis, Univeristy of Illinois at Urbana-Champaign, 2007.

[27] P. Y. Chan, N. Goldenfeld, and J. Dantzig, Phys. Rev. E **79**, 035701(R) (2009).

[28] P. F. Tupper and M. Grant, Europhys. Lett. **81**, 40007 (2008).

[29] G. Brambilla, D. El Masri, M. Pierno, L. Berthier, L. Cipelletti, G. Petekidis, and A. B. Schofield, Phys. Rev. Lett. **102**, 085703 (2009).

[30] W. Götze, *Complex Dynamics of Glass-Forming Liquids: A Mode-Coupling Theory* (Oxford University Press, Oxford, UK, 2009).

[31] W. Kob and H. C. Andersen, Phys. Rev. E **52**, 4134 (1995).

[32] C. W. Gardiner, *Handbook of Stochastic Methods for Physics, Chemistry and the Natural Sciences* (Springer-Verlag, Berlin, 2004).

[33] M. J. Robbins, A. J. Archer, U. Thiele, and E. Knobloch, Phys. Rev. E **85**, 061408 (2012).

[34] W. Kob and J. L. Barrat, Eur. Phys. J. B **13**, 319 (2000).

[35] J. L. Barrat and J. P. Hansen, *Basic Concepts for Simple and Complex Fluids* (Cambridge University Press, Cambridge, 2003).

[36] J. Berry, M. Grant, and K. R. Elder, Phys. Rev. E **73**, 031609 (2006).

[37] J. Berry, N. Provatas, J. Rottler, and C. W. Sinclair, Phys. Rev. B **86**, 224112 (2012).

[38] P. Y. Chan, G. Tsekenis, J. Dantzig, K. A. Dahmen, and N. Goldenfeld, Phys. Rev. Lett. **105**, 015502 (2010).